JOURNAL OF GEOPHYSICAL RESEARCH, VOL. 101, NO. A1, PAGES 241-259, JANUARY 1, 1996

Observations of thermospheric horizontal neutral winds at Watson Lake, Yukon Territory (Λ = 65°N)

R. J. Niciejewski and T. L. Killeen

Space Physics Research Laboratory, University of Michigan, Ann Arbor

Stanley C. Solomon

Laboratory for Atmospheric and Space Physics, University of Colorado, Boulder

Abstract. Fabry-Pérot interferometer observations of the thermospheric O I (6300 Å) emission have been conducted from an airglow observatory at a dark field site in the southeastern Yukon Territory, Canada, for the period November 1991 to April 1993. The experiment, operated in an unattended, remote fashion, has resulted in a substantial data set from which mean neutral winds have been determined. Dependent upon geomagnetic activity, the nocturnal location of the site is either equatorward of the auroral oval or within the oval boundaries. The data set is rich enough to permit hourly binning of neutral winds based upon the K_p geomagnetic disturbance index as well as the season. For cases of low geomagnetic activity the averaged, vector horizontal neutral wind exhibits the characteristics of a midlatitude site displaying antisunward pressure-gradient-driven winds. As the geomagnetic activity rises the late afternoon and evening winds slowly rotate sunward in an anticlockwise direction, initially remaining near 100 m/s in speed but eventually increasing to 300 m/s for $K_p > 5$. For the higher levels of activity the observed neutral wind flow pattern resembles a higher-latitude polar cap pattern characterized by ion drag forcing of thermospheric neutral gases. In addition, rotational Coriolis forcing on the dusk side enhances the ion drag forcing, resulting in dusk winds which trace out the clockwise dusk cell plasma flow. On the dawn side the neutral winds also rotate in an anticlockwise direction as the strength of geomagnetic disturbances increase. Since the site is located at a transition latitude between the midlatitude and the polar cap, the data set provides a sensitive test for general circulation models which attempt to parameterize the contribution of magnetospheric processes. A comparison with the vector spherical harmonic (VSH) model indicates several regions of poor correspondence for December solstice conditions but reasonable agreement for the vernal equinox.

Introduction

The upper thermosphere is the region which separates the interplanetary environment from the terrestrial domain and is consequently affected from above by solar-driven processes. Though relatively vacuous compared to the troposphere, the thermosphere is dense enough to support its own climate and weather patterns. The dynamical influence of solar heating tends to drive a pressure gradient wind from the subsolar point across the terminator towards the night side of the Earth. At high latitudes, terrestrial magnetospheric processes are important in determining the thermospheric wind flow primarily through momentum transfer from rapidly moving plasma. In addition, the inherent Coriolis forcing associated with the rotation of the Earth has an effect.

Long-term observational programs monitoring the neutral dynamics in the upper thermosphere at auroral latitudes have been performed directly via high-resolution optical methods or indirectly via incoherent scatter radar reflections. Ground-based optical experiments with a Fabry-Pérot interferometer were performed at College, Alaska (invariant latitude Λ = 65) [*Sica*, 1984; *Sica et al.*, 1986a] from which average neutral winds for low ($A_p \leq 11$), moderate, and high ($A_p \geq 39$) geomagnetic conditions were determined. A corresponding study by *Aruliah et al.* [1991a] discussed average neutral winds for different K_p conditions and low ($F_{10.7} \leq 100$), moderate, and high ($F_{10.7} \geq 170$) solar flux levels as observed at Kiruna (Λ = 65°). Seasonal effects on the magnitude of the upper thermospheric neutral winds have also been investigated at Kiruna [*Aruliah et al.*, 1991b]. In this latter study the influence of low ($F_{10.7} \leq 110$) and high ($F_{10.7} > 110$) solar flux levels during different seasons were also studied. Mean meridional winds have been derived from European incoherent scatter (EISCAT) (Λ = 67°) radar data as a function of season during solar minimum conditions [*Titheridge*, 1991]. This set is the only study which provides summer season wind measurements. Neutral winds have also been measured by a Michelson interferometer at Sodankylä and Tromsø (EISCAT radar sites) during short campaign runs between November 1988 and January 1991 providing similar conclusions as the Kiruna studies [*Fauliot et al.*, 1993]. Finally, *Crickmore* [1994] has presented a study of the mean upper thermospheric winds at Halley (Λ = 62°S) as a function of season, high ($\Sigma K_p > 24$) and low ($\Sigma K_p < 16$) geomagnetic activity, and high ($F_{10.7} > 190$) and low ($F_{10.7} < 144$) solar flux level.

Model descriptions of the upper thermospheric neutral winds have appeared for both empirical and theoretical studies

Paper number 95JA02683.
0148-0227/96/95JA-02683$05.00

Hedin et al. [1991] have collated a large number of satellite-borne and ground-based observations to generate the empirical horizontal wind model (HWM) description of global thermospheric dynamics. Theoretical simulations of thermospheric dynamics have been performed independently based upon two constantly improving models: the National Center for Atmospheric Research (NCAR) thermospheric general circulation model (TGCM) [*Dickinson et al.*, 1981] and the University College London (UCL) TGCM [*Fuller-Rowell and Rees*, 1980]. These models are typically difficult to use, which has led to the development of the VSH parameterized version of the NCAR model [*Killeen et al.*, 1987].

We report in this paper observations of upper thermospheric horizontal neutral winds based on a new detection technique, a Fabry-Pérot interferometer utilizing a "bare" CCD as the detector. The technique permitted instantaneous viewing of multiple copies of an O I (6300 Å) emission line profile thereby inherently increasing the signal-to-noise ratio over traditional single fringe measurements. Consequently, even though the experiment operated for only two dark observing seasons, a large amount of high-quality data was collected. These data sets provide an element towards the high latitude component of the coupling energetics and dynamics of atmospheric regions (CEDAR)-sponsored coordinated analysis of the thermosphere (CAT) program [*Hagan et al.*, 1991]. The results are comparable with the auroral zone observational studies described above, though with the greater density of data in the current study, it is now possible to simultaneously compare the thermospheric horizontal neutral wind as a function of both K_p and season, the former discriminant being much finer than ever previously conceivable.

Experiment

An airglow observatory, shown in Figure 1, was established in 1991 at a dark field site near Watson Lake, Yukon Territory (latitude: 60 N, longitude: 129°W). The instrument complement included a Fabry-Pérot interferometer, a Michelson interferometer, and an all-sky imager, the latter operated by Utah State University. In the present study, only data acquired by the Fabry-Pérot interferometer shall be discussed. This instrument operated in an unmanned, remotely controlled mode during two dark observing seasons: (1) November 1991 to April 1992 and (2) November 1992 to April 1993. The Fabry-Pérot observation program concentrated solely on acquiring measurements of the upper thermospheric O I (6300 Å) emission feature. Much of the construction of the Fabry-Pérot interferometer experiment resembled that described by *Meriwether et al.* [1983], but the detection system utilized a bare charge-coupled device and a microprocessor-controlled data acquisition system [*Niciejewski et al.*, 1994]. Operational parameters of the Fabry-Pérot interferometer are listed in Table 1.

The CCD chosen for the detector was the Kodak KAF1400 chip which was supplied hermetically sealed in a thermoelectrically cooled liquid circulation unit. The system ran in the multipinned phase (MPP) mode which reduced dark noise levels substantially. In addition, the individual detection elements (pixels) were co-added on chip to form 8-x-8-pixel-wide "super

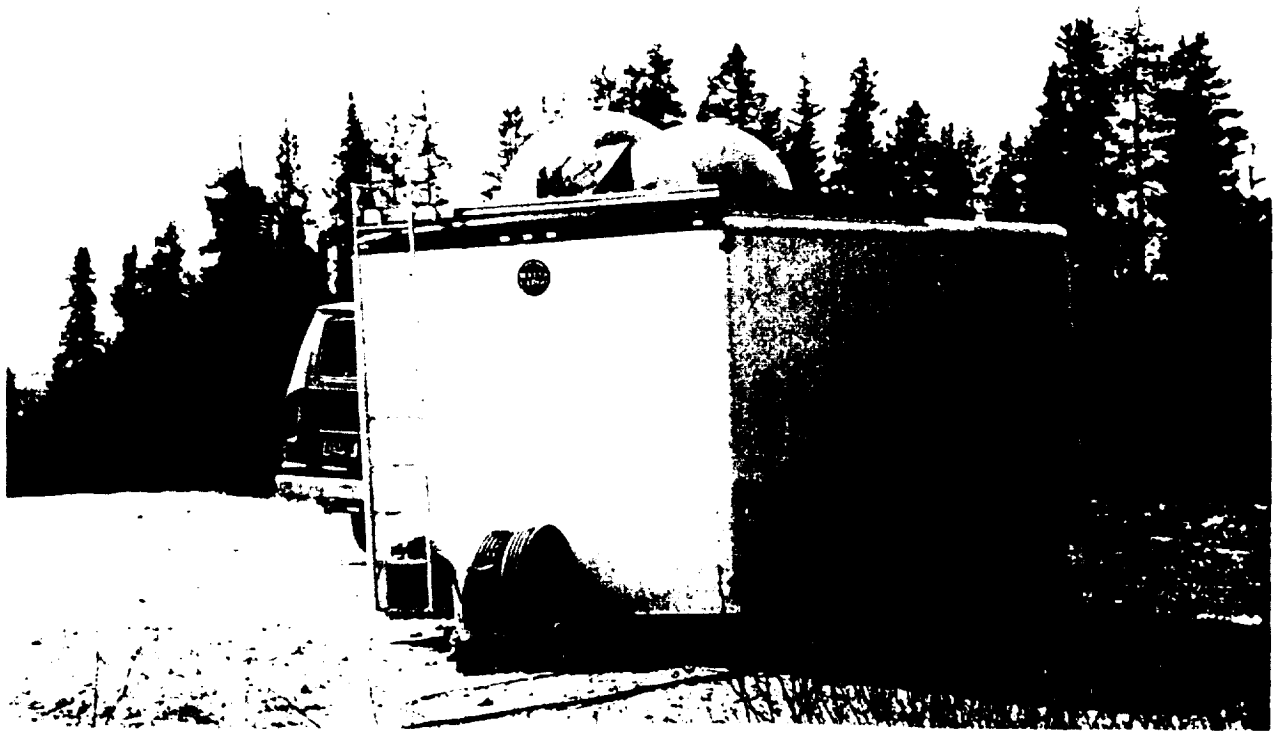

Figure 1. Photograph of the airglow observatory at the Watson Lake field site. The Fabry Perot interferometer resides on an optical bench beneath one of two transparent Plexiglass domes. The site is located on a mountain top about 10 miles (16 km) east of town.

Table 1. Operational Parameters for the Fabry-Pérot Interferometer at Watson Lake Airglow Observatory

Optics	Parameter
Etalon plates; reflectivity at 6300 Å*	91%
Clear aperture	12.5 cm
Spacer gap (solid annular quartz ring)	1.0 cm
Typical working finesse for innermost channel	14
Interference filter	
center wavelength	6300 Å
band pass	8 Å
transmission	70%

Lens	Diameter, cm	Focal Length, cm
Objective	15	155
Collimating	5	60
Condensing	5	10

The lens combination given above implies nearly three complete free spectral ranges at λ6328 Å imaged onto the detector. The free spectral range is 0.20 Å at λ6300 Å. The detector is a Kodak KAF1400 with 1317 x 1035 pixels (pixel size is 6.8 x 6.8 μm); readout noise, 11.2 e^- RMS; dark noise, 0.003 e^-/s at -42 °C.

* Manufactured by IC Optical Systems Ltd

pixels" prior to image readout in a successful effort to reduce readout noise. Using the lenses and filter described in Table 1, three O I (6300 Å) profiles, or fringes, were simultaneously imaged onto the detector. The integration period per sky image varied between 10 and 180 s based solely upon the O I (6300 Å) signal strength. The integration period was determined dynamically on site by the data acquisition controller based on an initial 10-s exposure. The criterion employed was to choose the shortest integration which would provide a wind error of approximately 5 m/s but not to observe more than 180 s in any direction. Instrumental drift of the Fabry-Pérot interferometer was monitored by frequently observing a Ne calibration lamp. Prior to the start of each of the two dark observing seasons, an instrumental calibration was performed with a frequency stabilized HeNe laser. Analysis of the drift measurements and the instrumental calibrations indicated that the local experimental environment remained stable during each season.

The routine patrol mode of operation of this experiment was to observe both the horizontal and vertical thermospheric wind by cycling through a series of five sky scans: a zenith-directed measurement to define the vertical wind, north- and south-directed measurements to define the meridional wind, and east- and west-directed measurements to define the zonal wind. The cardinal point scans were performed at a 45° elevation angle. Following each cycle, the raw images were reduced into wavelength space using the technique described by *Mulligan* [1986]. This provided fringe profiles from annular or ring-sum bins. Geophysical parameters were extracted from the multiple fringe profiles using a technique based on that of *Killeen and Hays* [1984]. These parameters were then both stored in the data logger as well as broadcast over a telephone modem line for instant viewing. Cloud cover information was obtained from the Watson Lake airport meteorological service at 1-hour intervals and later used to remove poor-quality data.

Results

Guided in part by the CAT analysis procedures, certain bin sizes and conditions have been chosen for studying the mean neutral horizontal wind. To describe seasonal influences on the neutral winds, the "December solstice" season was defined to include the 2 months December and January. Similarly, the "March equinox" season was defined as data accumulated during March and April. Unfortunately, no data were acquired during the autumnal equinox period and sky conditions were too bright for any June solstice measurements. The Fabry-Perot data sets thus provided four seasons for detailed study: December solstice, 1991; March equinox, 1992; December solstice, 1992; and March equinox, 1993. Since the solar cycle is much longer than the observation windows, no further filtering based upon the $F_{10.7}$ solar flux measurements was performed. Table 2 defines the solar flux values for the four seasons of study. Since Watson Lake can be both a subauroral and an auroral site, filtering based upon the geomagnetic disturbance index, K_p, was performed. As shall be demonstrated later, the effect of geomagnetic activity upon the neutral winds is quite noticeable. Finally, a bin width of 1 hour was chosen for the data study, based partly upon the frequency of cloud cover information and partly on the need for desirable statistics for the bins.

Auroral Contamination

A potential source of error in describing the mean upper thermospheric winds is the contribution of auroral emission to the measurement. This is a fault that is inherent to all ground-based optical diagnostic techniques which attempt to observe terrestrial airglow emission and is evidenced either through a particularly strong enhancement in the observed signal channel or through unwanted contributions from contaminating auroral-only channels, the latter summarized by *Gattinger and Vallance Jones* [1974]. There have been several studies describing an altitude change in the peak height of O I (6300 Å) emission during aurora [*Sica et al.*, 1986b; *McCormac et al.*, 1987a], indicating that a ground-based observation may actually be viewing emission weighted to a much lower altitude than during a "pure nightglow" case and subsequently possible contaminant for the present statistical study. Consequently, a simple technique was developed to exclude obvious auroral data from desired nightglow-only data.

The occurrence frequency of aurora have been studied for many years, and their geomagnetic time-latitude distributions for various levels of magnetic disturbance have been summarized by *Feldstein and Starkov* [1967]. Figure 2 displays a mathematical representation of the oval for different levels of the magnetic disturbance Q index (similar to the K index for auroral region stations) based on the formulae of *Holzworth and Meng* [1975]. Given the invariant latitude of Watson Lake (65) and that local magnetic midnight occurs at 9.65 UT, it is clear that the site is a "midlatitude" station for Q levels 0 and perhaps 2. At greater disturbance levels the site lies near the boundaries of the auroral oval.

Table 2. Mean Solar Flux Values for the Four Seasons of Study

Season	Solar Flux
December solstice, 1991	213.8
March equinox, 1992	164.7
December solstice, 1992	125.9
March equinox, 1993	125.8

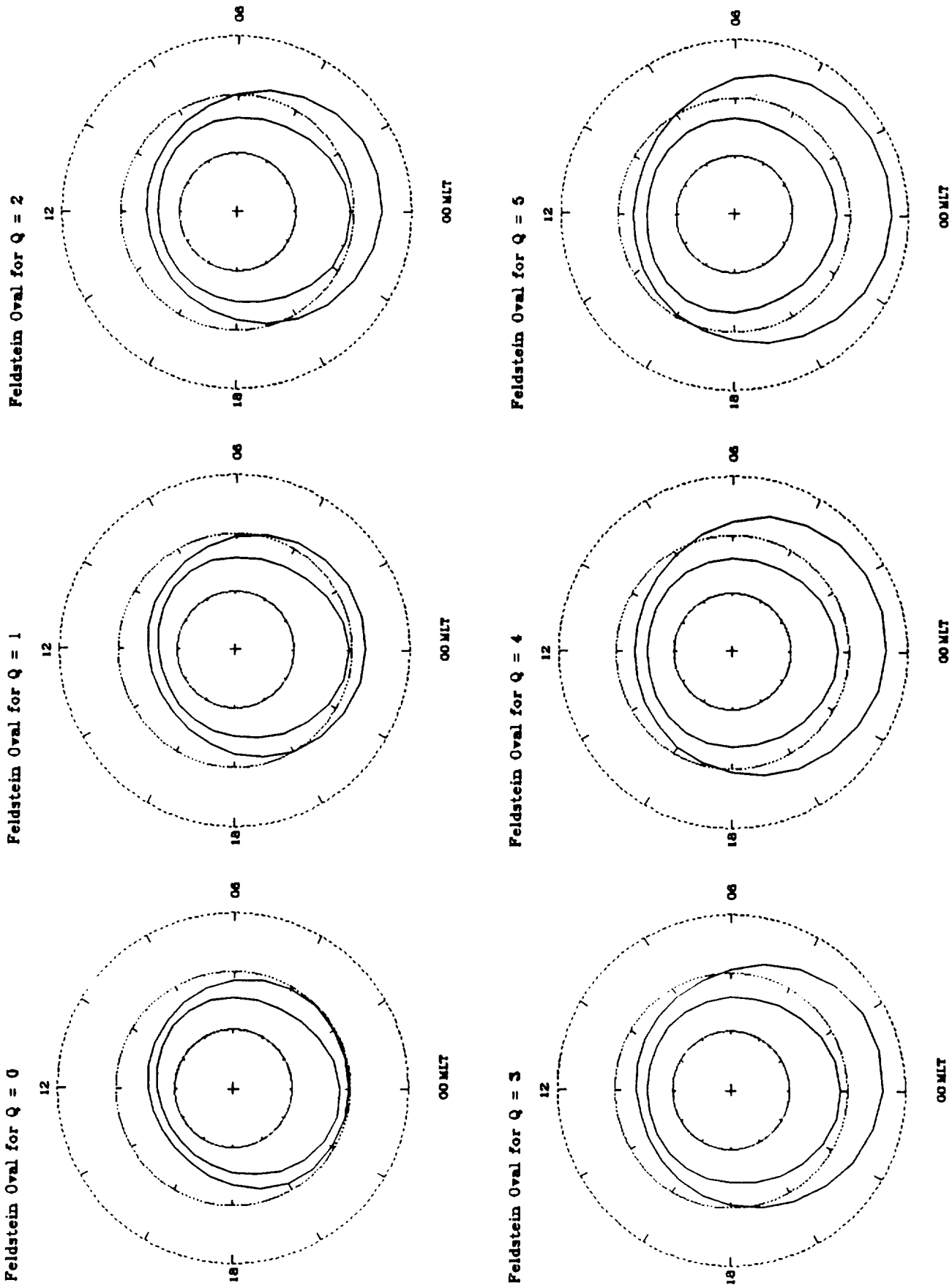
Feldstein Oval for Q = 0
Feldstein Oval for Q = 1
Feldstein Oval for Q = 2
Feldstein Oval for Q = 3
Feldstein Oval for Q = 4
Feldstein Oval for Q = 5
06
12
18
00 MLT

It is interesting to display the mean hourly binned O I (6300 Å) signal levels filtered according to the K_p index. For this analysis and for related analyses in the remainder of this report, measurements were sorted into bins 1 K_p unit wide, that is, $0 < K_p \leq 1$, $1 < K_p \leq 2$, etc., primarily because the auroral oval moves equatorward over Watson Lake rapidly as geomagnetic activity increases. Figure 3 displays the average signal levels with their corresponding standard deviation values for the December 1992 solstice period. There are several common features evident in this series. The evening twilight decay of the O I (6300 Å) signal reflects the approximately 1-2-hour time constant for the decay of the plasma densities in the F region since, in the absence of auroral precipitation, the excited O(^{1}D) state is primarily populated via dissociative recombination of O_2^+ and e^-. As a corollary, the morning twilight enhancement is a much more rapid event. A magnetic midnight enhancement in signal level is evident for all levels of geomagnetic activity. For K_p index levels greater than 2, a marked asymmetry in signal level about magnetic midnight exists. This latter behavior is likely resultant from the skewing of the auroral oval to the postmagnetic midnight hours as displayed in Figure 2. Finally, it is clear that the mean signal levels rise in intensity as geomagnetic activity rises, though only by factors of about 5 rather than by orders of magnitude.

The behavior of the average signal level is similar for the higher solar flux December 1991 solstice period. The primary difference is that the signal level is greater in magnitude, as would be expected, since the plasma density which drives the dissociative recombination reaction is greater. An interesting anomaly is that the signal levels for the magnetic midnight periods for $K_p > 3$ actually are decreased with respect to pre- and postmidnight periods. A less obvious behavior is evident for the corresponding period in Figure 3. In both cases it is possible that the equatorward edge of the oval has descended so far south that Watson Lake is entering the polar cap. The average signal plots for the vernal equinox seasons are similar though shorter in duration. The signal enhancement at magnetic midnight for low-K_p conditions is present, as well as the asymmetry in signal levels about magnetic midnight. Signal levels also increase as geomagnetic activity increases.

To estimate the contribution to the 6300-Å signal from auroral contributions, an auroral ionization (GLOW) [*Solomon*, 1993] model was run. This model calculates ionization and excitation rates, energetic electron production and transport, excited species densities, and airglow emission rates based upon solar and geomagnetic input parameters. The neutral atmosphere is modeled by the mass spectrometer/incoherent scatter (MSIS) model and the ionosphere description is obtained from the international reference ionosphere (IRI) model. To simulate the background O I (6300 Å) airglow, a run was made for December solstice, $A_p = 5$ (approximately $K_p = 1.5$) and is displayed in Figure 4a. Here, the general features witnessed in the Watson Lake observations are present: the slow dusk intensity decay, the rapid dawn brightening, the increase in signal strength as solar flux increases, and the magnetic midnight enhancement observed for the low-K_p cases. The midnight feature arises from an increase in the IRI-modeled F region plasma density near the peak altitude of O I (6300 Å) emission. This occurs at approximately the time that the Harang discontinuity passes over Watson Lake, that is, the boundary between the dusk and dawn plasma convection cells where the plasma flow is primarily and strongly antisunward. Runs were then made for various simulated aurora: Figure 4b displays the resultant O I (6300 Å) emission for an aurora characterized with a mean energy of 1 keV and an energy flux of 1 erg cm^{-2} s^{-1}. As expected, the resultant emission is enhanced due to the auroral precipitation, in this case by more than an order of magnitude during dark night conditions.

Subsequently, Figure 5 displays the mean signal levels of Figure 3 but in a histogram representation. Here, each hourly bin of reported signal measurements have been additionally binned according to the relative value: 0 to 5 units, 5 to 10 units, etc., and then displayed centered upon the hour of the bin. The vertical scale has been normalized to the maximum histogram depth. As the geomagnetic index increases, the population of the bins slowly changes towards a bimodal distribution with the largest proportion of contributors in the first two bins (0 to 5 and 5 to 10) and then an occasional minor peak corresponding to the higher intensity levels. For the purpose of excluding purported auroral O I (6300 Å) contributors to neutral wind bins, measurements corresponding to signal levels greater than 10, a conservative value suggestive of the maximum airglow-dominated level, have been excluded from the reported averages.

Neutral Wind Observations

The meridional winds for the December 1992 solstice period are displayed in the series of plots in Figure 6. The convention for positive winds chosen for the display is north and east positive. The mean winds with associated one-sigma standard deviation vertical bars are displayed for each hour of available measurement. For geomagnetic indices greater than 4, there were insufficient data points during certain hourly bins; these are consequently left blank. In addition, as the disturbance level increases, the hour of peak equatorward wind shifts from local midnight to predawn, though the magnitude does not increase appreciably until the highest disturbance levels. The behavior of the mean zonal winds is more complicated. As the disturbance level increases, the zonal wind changes from a predominantly eastward wind to one with a more diurnal nature: westward in the evening and eastward in the morning.

An alternate form for displaying the horizontal winds is to construct a vector wind and display such on a polar dial coordinate system. Figure 7 displays the neutral horizontal wind using a geomagnetic latitude-magnetic local time format. In this format the Sun is towards the top of the panels, magnetic midnight occurring at 9.65 UT at Watson Lake's position (invariant latitude is 65°N). The central cross is the magnetic pole with concentric circles surrounding it corresponding to latitudes 80°, 70°, and 60° respectively as the radii increase. The wind magnitudes are normalized to the barbed arrow at the bottom right. Each measurement is shown with the tail located at 65°N and the barb pointing in the prevailing wind direction, that is, the azimuth angle of the horizontal wind vector. As the disturbance level increases, the wind direction changes sub-

Figure 2. Feldstein ovals for various levels of the Q magnetic disturbance index. The polar plots have been constructed for geomagnetic latitudes 60° to 90° and as a function of magnetic local time. Watson Lake has an invariant latitude of 65°, and magnetic midnight occurs at 9.65 UT.

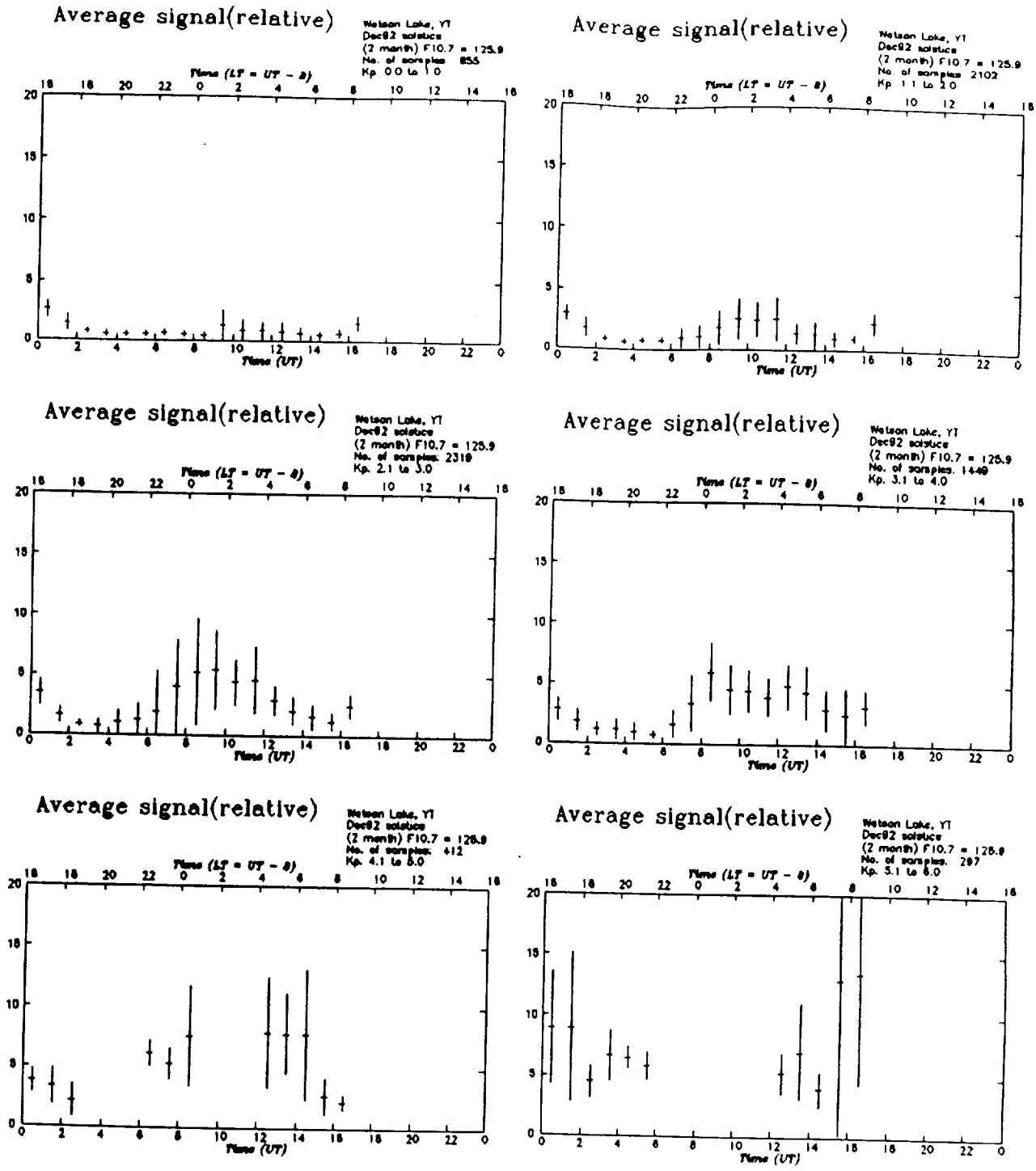

Figure 3. Mean O I (6300 Å) signal levels during the December 1992 solstice period. One-sigma standard deviation is also shown with each hourly mean. Binning was performed for unitarily increasing K_p indices.

stantially. Initially, the evening winds are directed in an antisunward direction roughly towards 0200 MLT. As geomagnetic activity increases, the winds slowly rotate in a counter-clockwise (from above) direction until, at the highest level, they are roughly tangential to the 65° latitude arc. During the morning hours, the wind vectors also rotate counter-clockwise with their magnitude increasing substantially.

Polar dial wind constructions for the March 1992 equinox appear in Figure 8. The evening and premidnight winds also follow a counter-clockwise rotation as the magnetic disturbance level increases and do so to a greater extent than during corresponding hours of the December solstice. During the morning hours, the rotation is also coupled with a substantial increase in the magnitude of the horizontal wind.

The neutral winds during the December 1991 period are similar to those shown in Figure 7. However, the general appearance of the polar dial displayed winds in Figure 9 show that the behavior is different by roughly 1 K_p index unit. Note that the

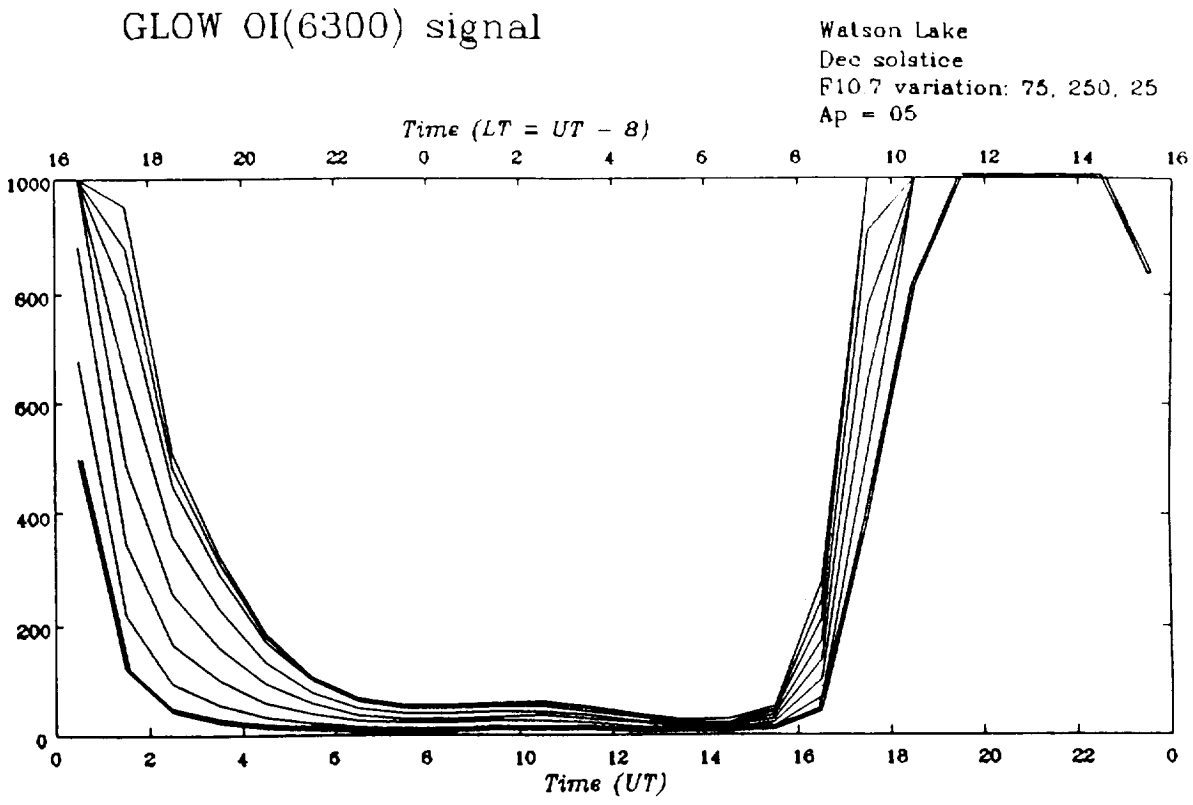

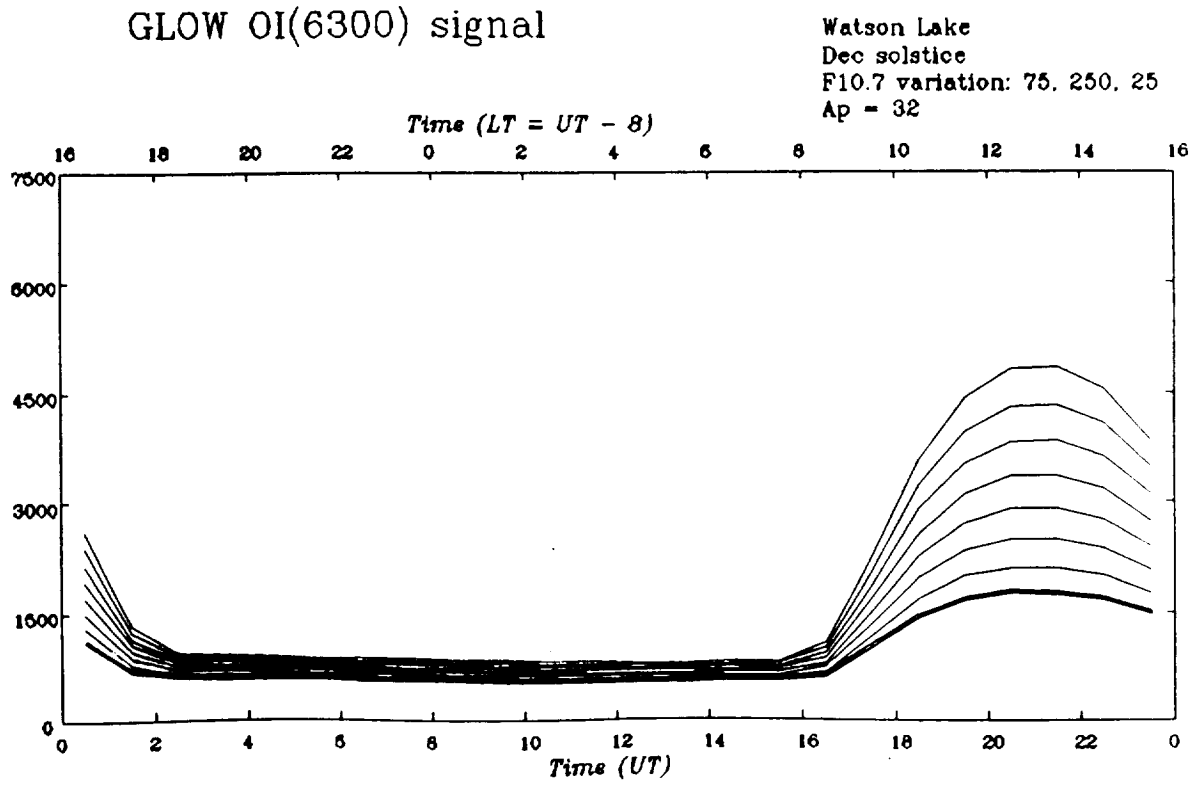

Figure 4. GLOW model output of the O I (6300 Å) intensity for December solstice, A_p = 5, for various solar flux levels ranging from $F_{10.7}$ = 75 (heavy line) to $F_{10.7}$ = 250 in increments of 25 $F_{10.7}$ units. (a) Photochemistry only, no aurora; (b) with an aurora of mean energy 1 keV and energy flux of 1 erg cm^{-2} s^{-1}.

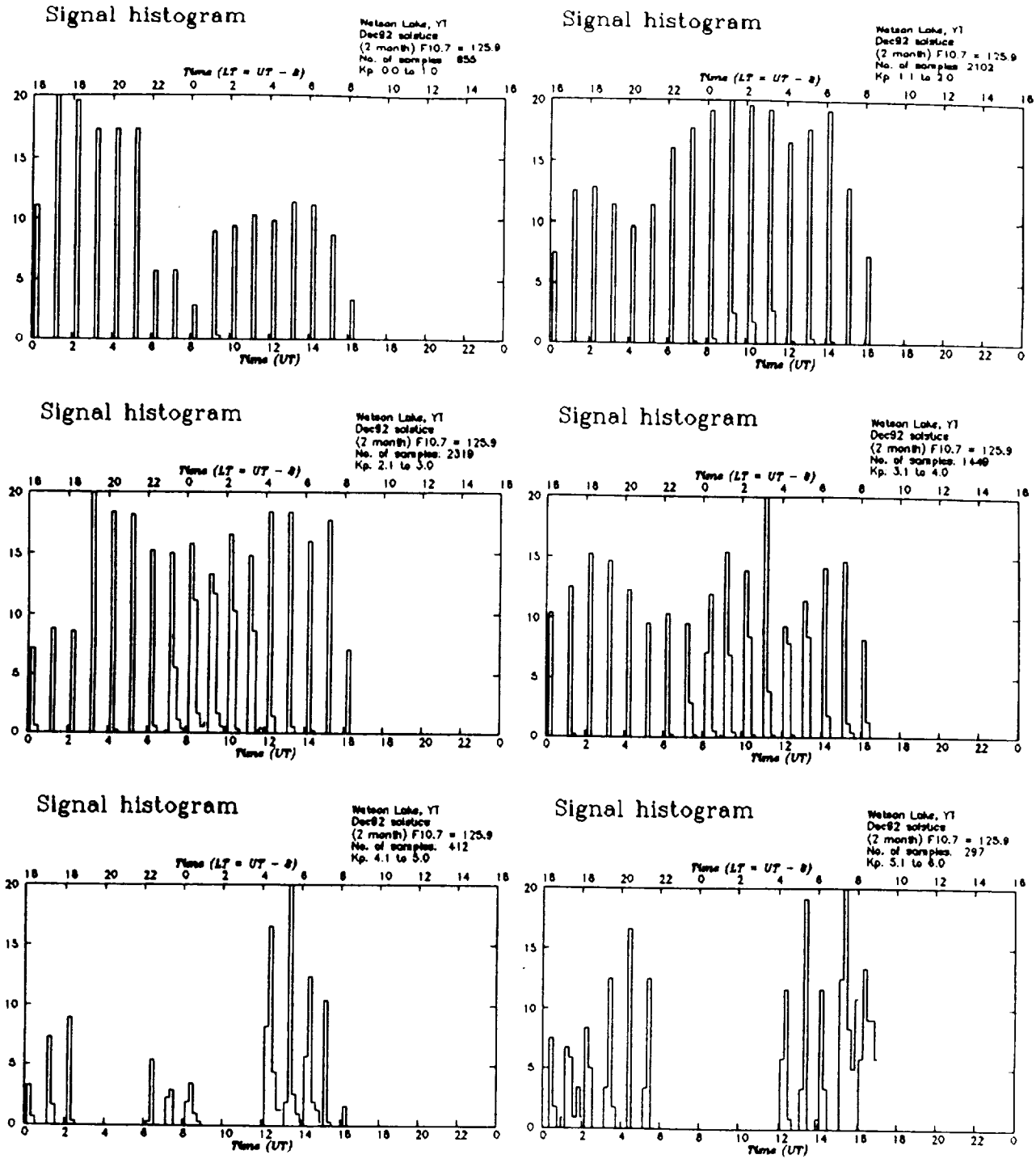

Figure 5. Signal level data of Figure 3 but displayed in a histogram form. Each hourly bin of Figure 3 was further subdivided based on the strength of the signal level: 0 to 5, 5 to 10, etc. The resulting distributions are displayed normalized to the peak bin population for each K_p level and ordered about the hour of the measurement.

solar flux values for the two solstice periods correspond to a solar maximum level for late 1991 and low to moderate for late 1992. Finally, the March 1993 horizontal winds shown in Figure 10 are very similar in appearance to those acquired a year earlier. The primary difference is that the magnitude of some of the wind vectors is diminished.

Neutral Wind Model

The vector spherical harmonic (VSH) model, mentioned earlier, was used to assess the current theoretical understanding of the horizontal neutral winds at a subauroral/auroral site in comparison to the observations. The version employed for the

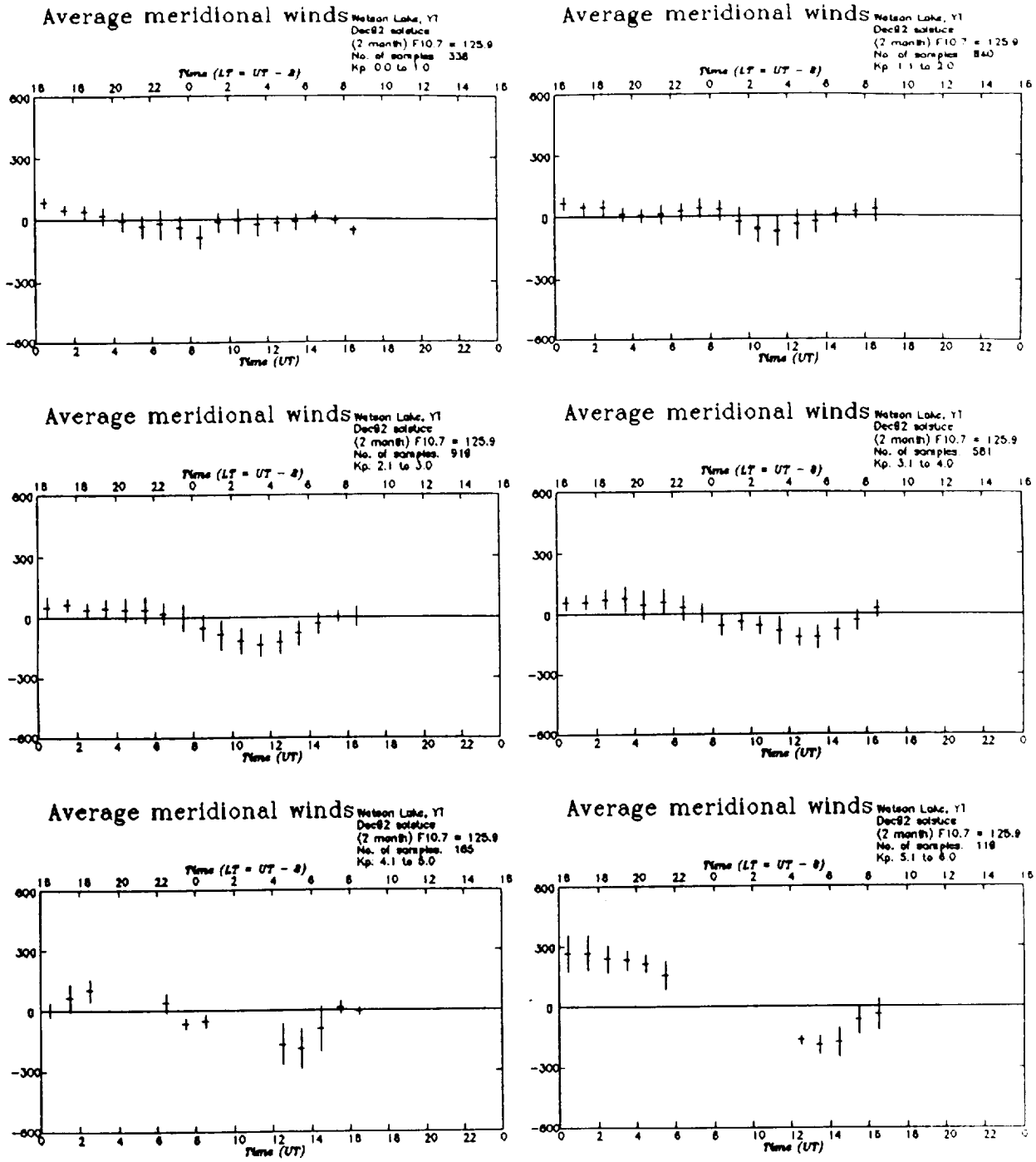

Figure 6. Neutral wind data for the December 1992 solstice period. (a) Meridional winds ordered with north positive; (b) zonal winds ordered with east positive. Mean wind values are shown with plus or minus one-sigma standard deviation vertical bars.

comparison smoothly summarizes the output from 18 different NCAR TGCM computer runs by a series of spectral coefficients for a total of 13 different geophysical parameters as a function of time, position, and disturbance and activity levels. The basis set of TGCM runs were acquired using a global grid ordered at 5°x5° in latitude and longitude, at 0.5 scale height in altitude, and at 5 min in time and were run until diurnally reproducible results were apparent. Runs were made for both the June and December solstices, as well as for a general equinox date. Different runs were evaluated for geomagnetic disturbance levels using A_p indices of 5, 11, and 32 (K_p values of roughly 1.5, 2.5, and 4.25) as well as for high ($F_{10.7}$ = 215) and low ($F_{10.7}$ = 72) solar activity cases.

Figure 11 displays the VSH model neutral wind simulation using the geomagnetic latitude-magnetic local time coordinate system for December solstice conditions, $F_{10.7}$ = 125, and a range of A_p indices. The solar flux value and the season describe the December 1992 solstice period. The range of A_p indices includes the three for which TGCM runs were performed as well as an extrapolation to A_p = 0. Though the VSH runs re

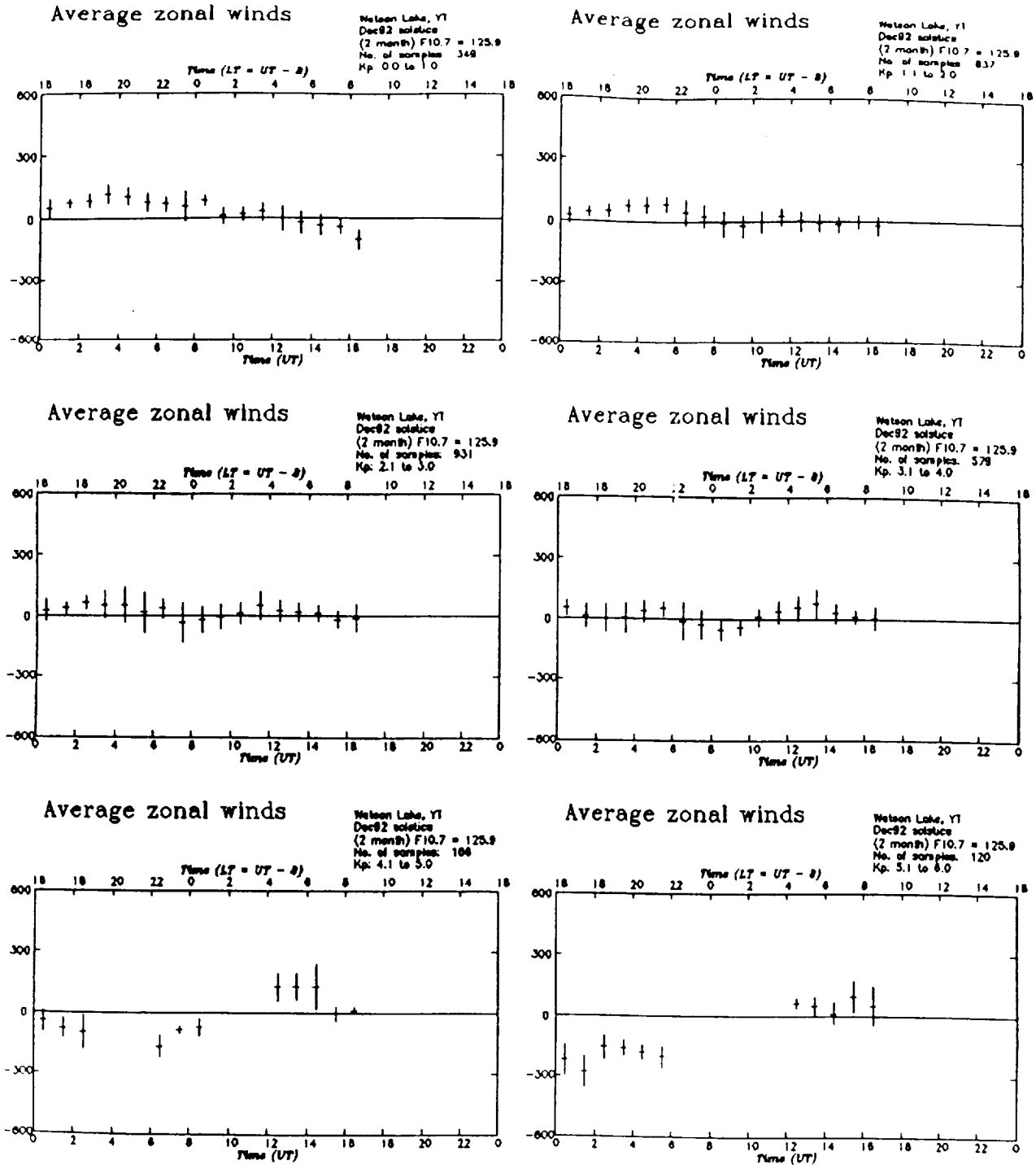

Figure 6. (continued)

quire geographic latitude-longitude inputs, the corresponding geomagnetic latitudes chosen for the simulation were 55°N, 65°N, and 75°N, all with a corresponding magnetic local midnight equal to that at Watson Lake. The model predicts that as the geomagnetic disturbance level increases, the horizontal wind vectors rotate in a counter-clockwise fashion in the noon to dusk and dusk to midnight sectors. Between midnight and dawn the wind primarily increases in magnitude as the index level rises, with some anticlockwise rotation nearest to 0600 MLT for lowest latitudes. The dawn to noon sector (an area unobservable from Watson Lake) indicates a strengthening in the antisunward flow across the pole as activity increases, along with a southward extension of the polar cap influence.

Figure 12 contains the results for the simulation corresponding to the March 1992 equinox period generated with a solar flux level of 175. The wind vectors are, in general, similar to corresponding vectors in Figure 11. Concentrating solely upon the 65° circle of wind vectors, the primary differences between Figures 11 and 12 occur in the postdusk period for the lowest A_p level and in the postmidnight hours for the higher disturbance levels. In particular, the horizontal wind magnitudes between 0000 and 0300 MLT are significantly en-

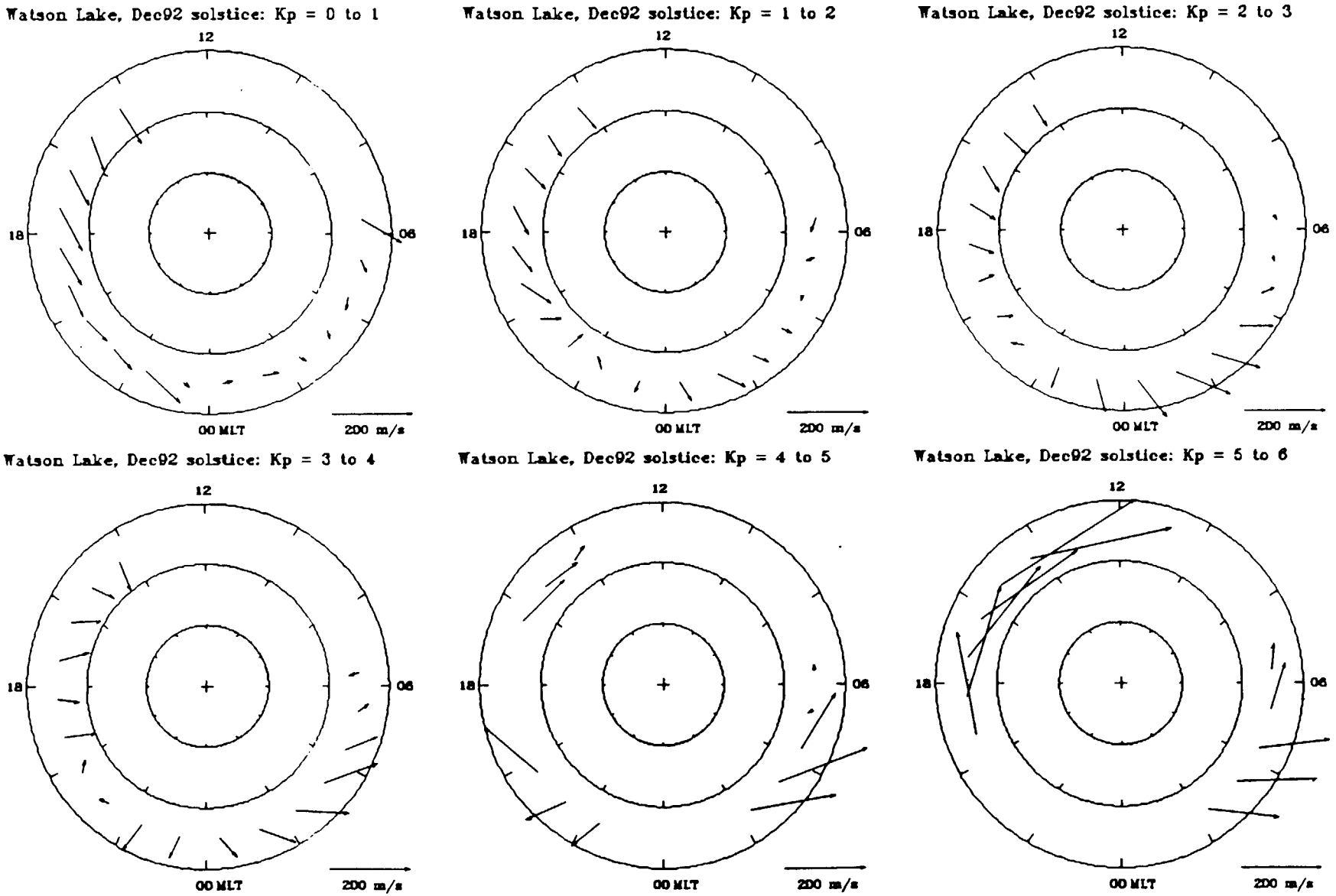

Figure 7. Neutral wind data for the December 1992 solstice period shown employing a polar dial representation. Here, the coordinate system is geomagnetic latitude and magnetic local time, where Watson Lake is at 65°N with magnetic local midnight at 9.65 UT. The length of the wind vector constructions are normalized to the 200 m/s barb appearing at lower right. The pointing direction of the wind vector construction corresponds to the azimuth angle of the horizontal wind. The outermost concentric circle corresponds to 60°, with the magnetic pole in the centre.

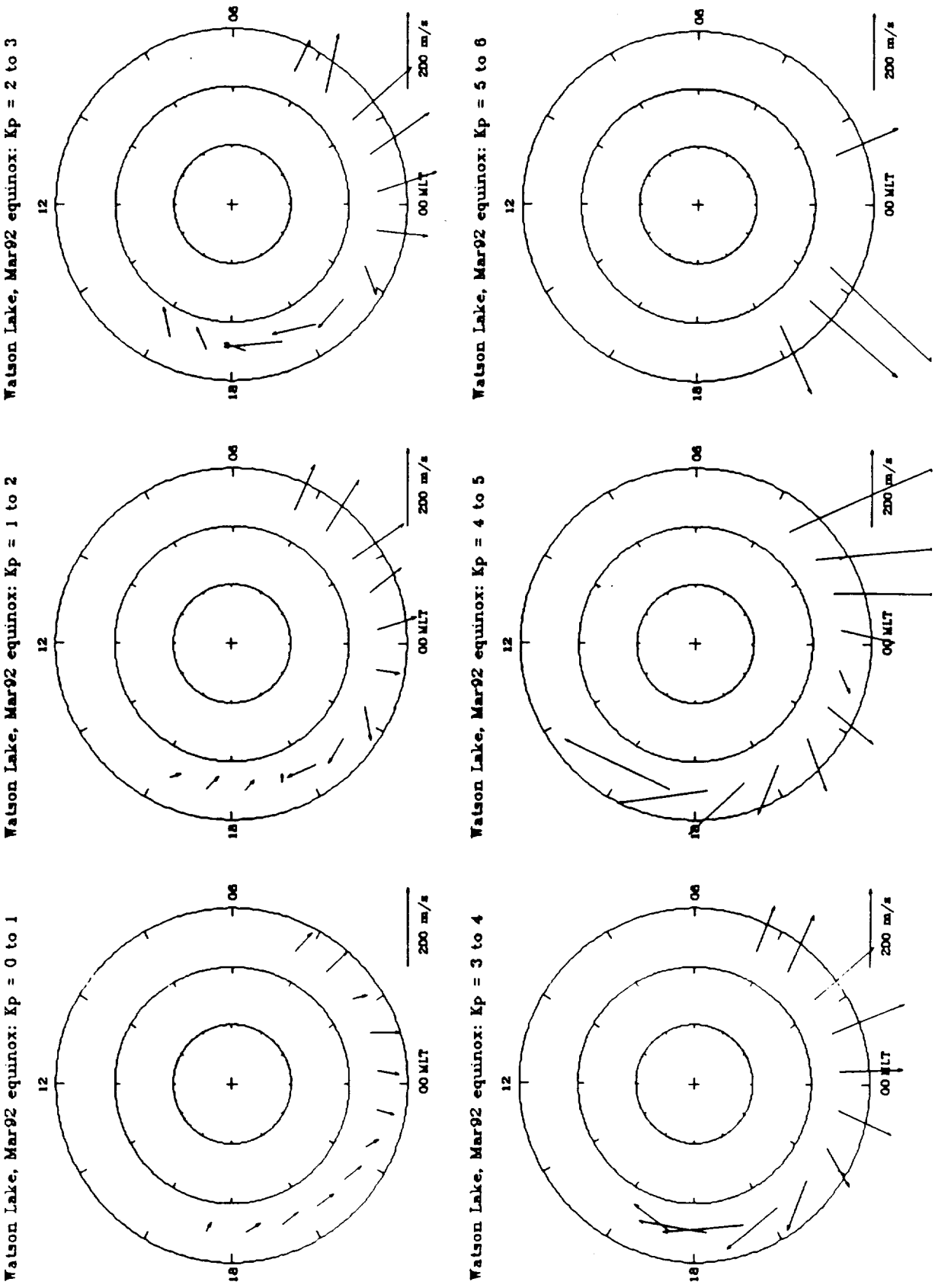

Figure 8. Neutral wind data for the March 1992 equinox period using the geomagnetic latitude-magnetic local time coordinate system.

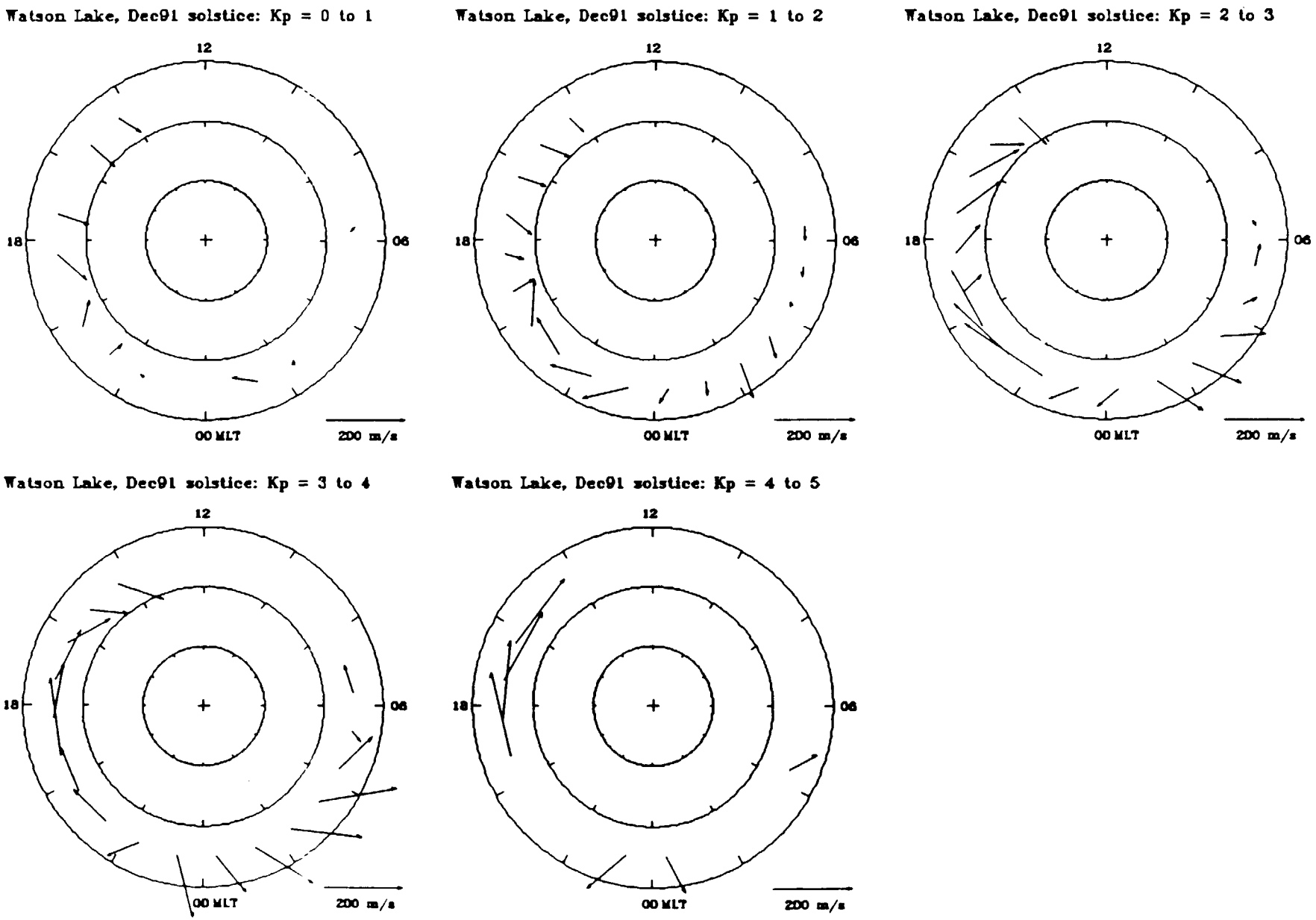

Figure 9. Neutral wind data for the December 1991 solstice period using the geomagnetic latitude-magnetic local time coordinate system.

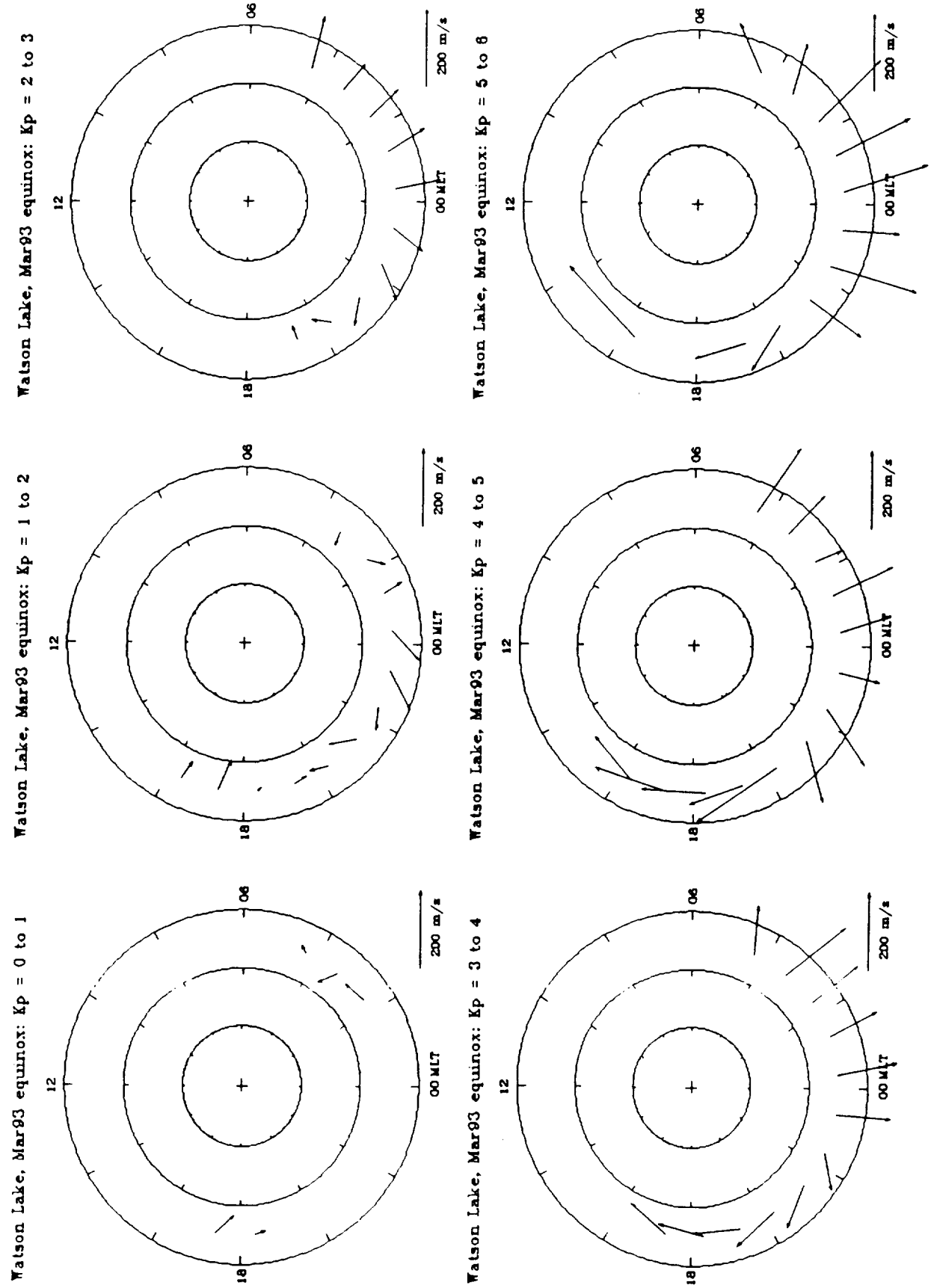

Figure 10. Neutral wind data for the March 1993 equinox period using the geomagnetic latitude-magnetic local time coordinate system.

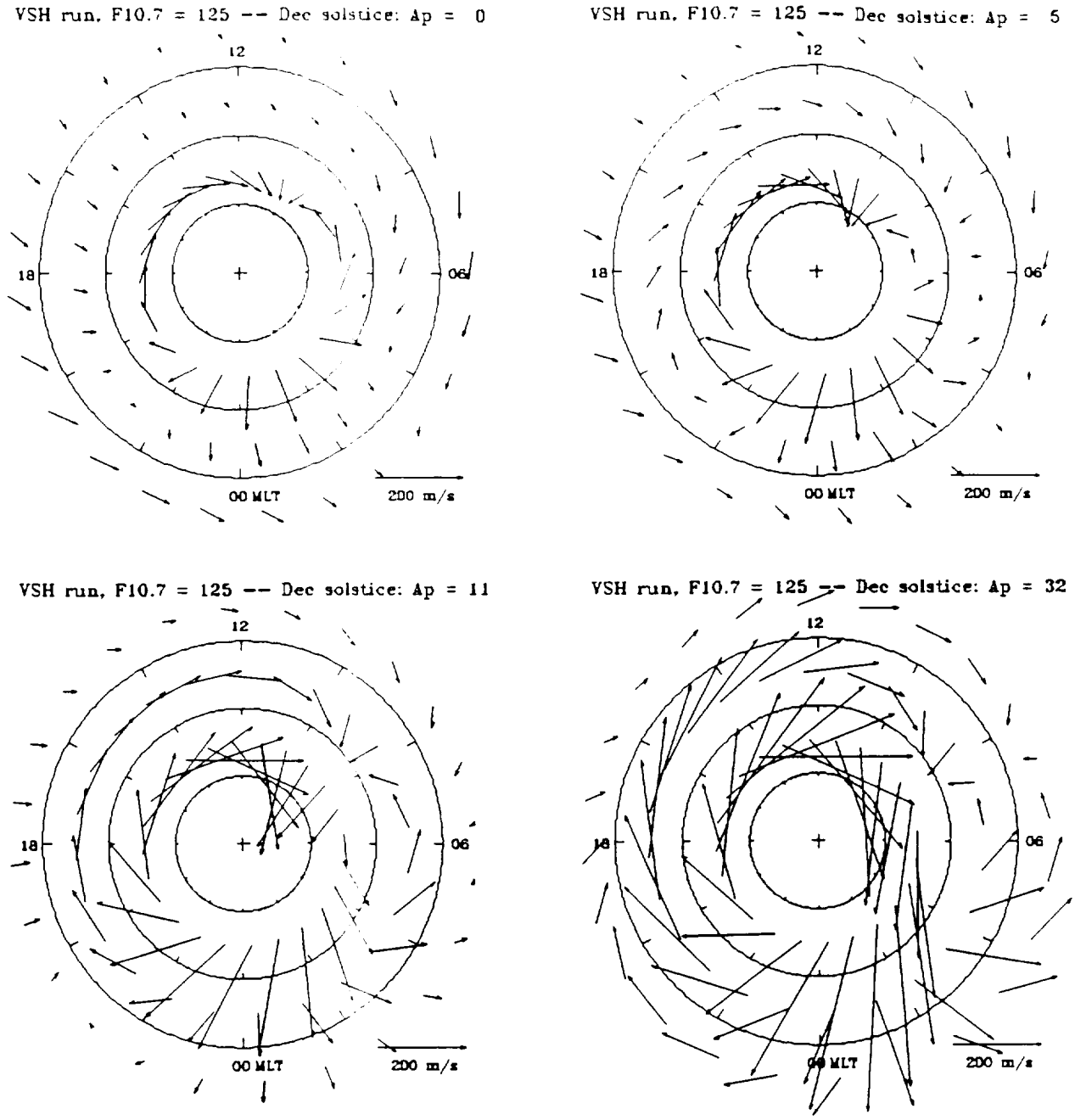

Figure 11. Neutral wind simulation for conditions reproducing the December 1992 solstice shown in a geomagnetic latitude-magnetic local time coordinate system. The coordinates for the simulated sites corresponded to magnetic latitudes 55°N, 65°N, and 75°N, all with a local magnetic midnight similar to Watson Lake's.

hanced in the equinox simulation. Finally, the behavior of the neutral winds at 65°N for simulations corresponding to the December 1991 solstice ($F_{10.7}$ = 225) and the March 1993 equinox ($F_{10.7}$ = 125) are similar to those developed for the December 1992 solstice and the March 1992 equinox, respectively, and are not shown in this report. As expected, the earlier solstice winds, simulated for a higher solar flux level, are typically greater in magnitude, but roughly similar in direction. Similarly, the later March equinox period corresponds to a lower solar flux level and consequently lower magnitude horizontal neutral winds in the simulation. For December solstice conditions, the greatest neutral horizontal winds simulated for 65°N occur postdusk at the highest geomagnetic disturbance value (A_p = 32), are greater than 300 m/s in magnitude, and are directed sunward. For March equinox conditions, the period following local magnetic midnight contains the greatest winds, also of magnitude greater than 300 m/s but directed antisunward.

Discussion

Watson Lake resides at a transitional boundary of thermospheric flow patterns, and consequently, long-term observations of mean thermodynamic characteristics are essential in

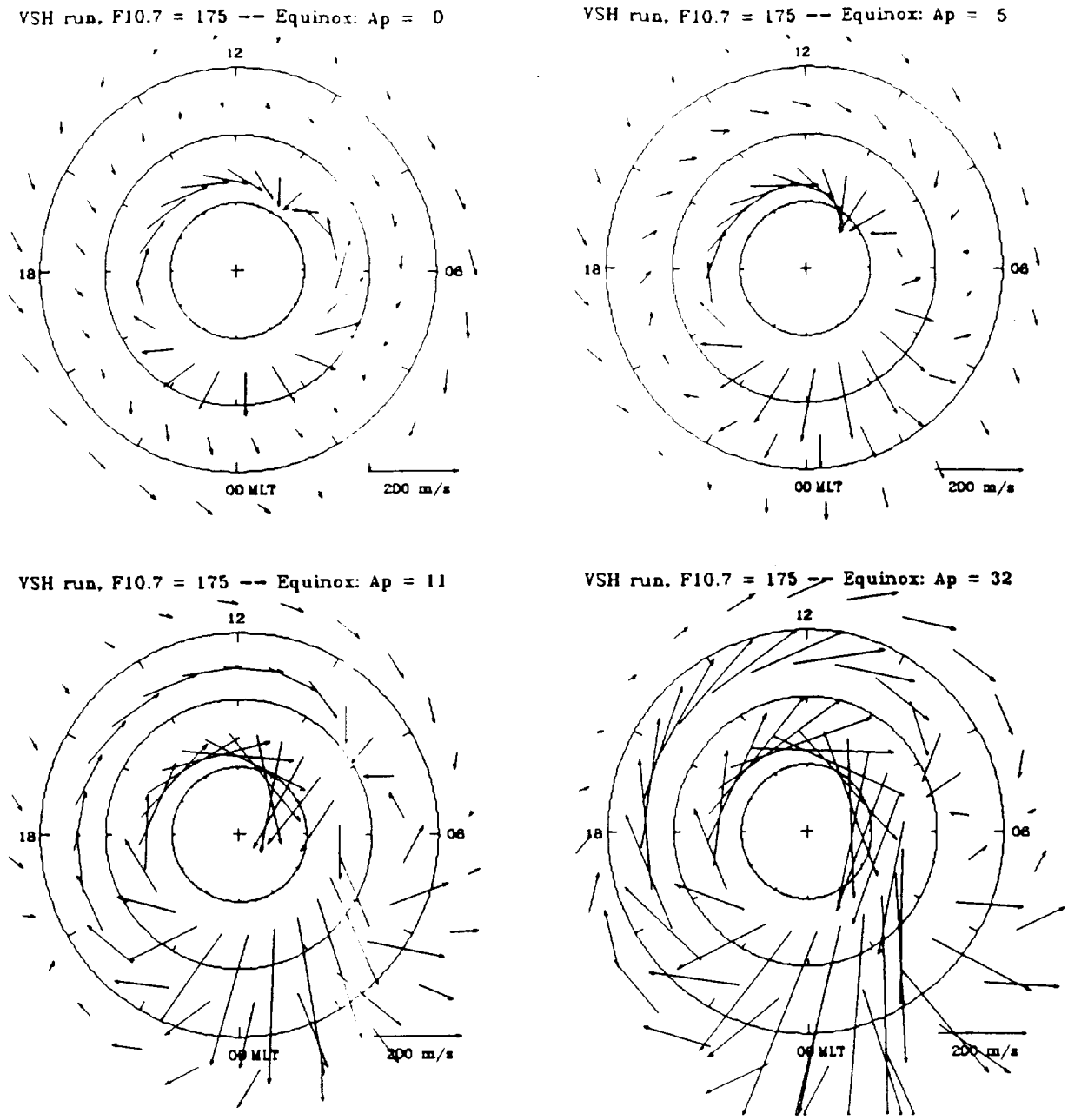

Figure 12. Neutral wind simulation for conditions reproducing the March 1992 equinox period shown in a geomagnetic latitude-magnetic local time coordinate system.

refining current understanding of global circulatory climatic models. The plasma density in the upper thermosphere is sufficient to forcefully drive neutral flow patterns if solar and magnetospheric processes perturb and accelerate the plasma drifts. The polar regions are open to the greatest plasma perturbations and through momentum transfer between collisions of neutral species and ions, the polar regions are also susceptible to "weather modifications" in the neutral thermosphere.

The current study has shown that the neutral winds at 65°N magnetic latitude are highly susceptible to modification as the planetary geomagnetic disturbance level varies. The K_p dependence in the meridional winds, shown in Figure 6, indicates that the hour of peak equatorward wind changes by 5 hours from $K_p = 0$ to $K_p = 5$. The magnitude change is not as dramatic, with the peak equatorward wind remaining at 100 m/s between $K_p = 0$ and $K_p = 2$, rising to 150 m/s from $K_p = 2$ to $K_p = 4$, and then peaking at 250 m/s between $K_p = 4$ and $K_p = 6$. As the disturbance level rises, the postdusk poleward wind increases in magnitude from 50 to 250 m/s. The zonal wind behavior is much more complicated, changing from an apparently diurnal variation at the lowest disturbance level, through an oscillatory behavior at middisturbance levels, back to an apparently diurnal behavior at the highest K_p levels though in antiphase with the lowest disturbance level. Consequently, it is not appropriate to characterize the wind components at this site simply by their maximum values as may be done for the highest polar latitudinal studies [*McCormac et al.*, 1987b], since it is clear that the peak zonal wind magnitude actually decreases with increasing disturbance level before it increases at the higher K_p levels.

The VSH wind field pattern displayed in Figure 11 for December solstice, a low solar to midsolar activity level, illustrates that two separate wind patterns are mixed at high latitudes. A predominant antisunward flow seen at equatorward latitudes for the lowest disturbance levels is driven by the pressure-gradient force directed from the warm sunward side to the colder night side of the Earth. At the highest latitudes the wind pattern consists of a two-cell structure split approximately along the noon-midnight meridian. As geomagnetic activity increases, the flow at 65°N changes from the pressure-gradient form at $A_p = 0$ to the two-cell flow at $A_p = 11$, resembling the flow at 75°N for $A_p = 0$. At this higher disturbance level, the flow at 75°N has changed significantly from that at $A_p = 0$. This new flow at 75°N also resembles the flow at 65°N when A_p is increased to its highest level. To summarize, the dominant flow at 65°N simulated by the VSH model changes character from pressure-gradient driven to ion drag-driven as A_p increases from 0 to 32, though the former does not truly disappear at the higher activity level.

The degree of correspondence between the measurements in Figure 7 and the VSH simulation in Figure 11 for 65°N depends on the time period examined. Between 1200 and 1800 MLT, the observed wind direction for $K_p = 0$ is similar to the $A_p = 0$ simulation, but the observed magnitudes are significantly greater. In fact, the observed winds do not begin to change direction until the K_p level exceeds 3, unlike the simulated change at $A_p = 5$ ($K_p \sim 1.5$). At the highest K_p levels the observed winds do follow the simulation for $A_p = 32$ quite well. Between 1800 and 0000 MLT there is no correspondence between observed winds at $K_p = 0$ and the simulated $A_p = 0$ winds at 65°N. However, the VSH simulation for 55°N strongly resembles the observed winds. The observed winds for K_p levels greater than 1 and less than 4 somewhat resemble the simulated curl in the VSH winds for 65°N. Once again, the observed winds for the highest disturbance levels correspond well with the $A_p = 32$ simulation. For the period 0000 and 0600 MLT, the correspondence between observations and simulations is quite good. In particular, the observed decrease in the wind intensity and the convergence at 0300 MLT for $K_p = 0$ is well simulated in the $A_p = 0$ case. The observed counter-clockwise rotation and enhancement in magnitude as K_p increases is well matched by the VSH model runs. Apparently, the VSH simulation is best during predawn but significantly underestimates the inertia of the pressure-gradient force between dusk and midnight unless one shifts the simulation latitude equatorward.

Regarding the March 1992 time frame, the observations in Figure 8 cover about 4 to 5 hours less of the diurnal cycle than those during the winter solstice. However, it is still valuable to compare with the VSH output of Figure 12 excluding the period 0500 to 1600 MLT. In fact, the comparison between observation and simulation is quite favorable to the simulation. The behavior in the observed winds between 1800 and 0000 MLT for $K_p = 0$ is more similar to the VSH run at $A_p = 0$ for 55°N in terms of magnitude, but closer in direction to the 65°N run. As the K_p level increases, the observed rotation in the wind vectors is predicted quite well by the equivalent VSH runs. For the period 0000 to 0600 MLT, the winds for the lowest disturbance observation are not well matched by any of the VSH runs, but as the K_p level increases, the predicted winds for the higher A_p levels match reasonably well in direction and magnitude.

The observations in Figure 9 correspond to a high level of solar activity. The corresponding VSH run (not shown here) strongly resembles that of Figure 11 except for an increase in magnitude in most wind vectors. However, most of the comments relating to the comparison of December 1992 solstice observations and the VSH runs for $F_{10.7} = 125$ also apply here. In particular, between 1200 and 1800 MLT, the observed winds for $K_p = 0$ are still greater in magnitude than those simulated even though the directions are approximately correct. Observations as the K_p level increases do not match the 65°N VSH circle for higher A_p levels until the highest K_p levels are reached. The correspondence from 1800 to 0000 MLT is much better for the December 1991 solstice as is the agreement with winds observed from 0000 to 0600 MLT. Finally, the observations in Figure 10 match quite well with a VSH simulation for $F_{10.7} = 125$. The only visible differences between the modelled and the observed winds are that occasionally the modelled winds are too high in magnitude.

The subtle differences for a constant geomagnetic disturbance level witnessed in the horizontal winds displayed in Figures 7 to 10 between different seasonal representations and the same season but a different solar flux level indicate that the interplay between different forcing mechanisms is complex. In general, the observed trend that the horizontal winds at 65°N evolve from a midlatitudinal to a polar cap flow as magnetic disturbances increase is repeatable for both the equinoctial and solstice seasons, but there are subtleties that cross the binning strategy employed in this study. For example, for $K_p = 3$ to 4, the horizontal winds observed during the two December solstices are significantly different (solar flux levels are quite different), but the two March equinox winds are similar (solar flux also different) and similar to the December 1991 solstice. This likely indicates that binning strategies for reporting mean winds need to be quite fine. Comparisons of the current data set with previously published data sets confirm this point. *Aruliah et al.* [1991a] binned neutral winds according to K_p index and solar flux level, but ignored seasonal differences. Consequently, even though the general trend in wind evolution is common to both data sets, fine details are not common; for example, for $K_p = 0$ to 1, Kiruna winds demonstrate very low magnitude winds during dusk and magnetic midnight with highest amplitude near 0300 MLT for both solar minimum and maximum, while Watson Lake winds, during December 1992 solstice, are strongest at dusk and weakest post midnight and during March 1992 equinox weakest at dusk and strongest post midnight. Seasonal differences are described by *Aruliah et al.* [1991b] but unfortunately at the expense of K_p binning.

The neutral wind data set described by *Sica et al.* [1986a] was acquired during a mix of seasons and solar activity levels and is coarsely divided into three different geophysical activity cases. In general, the trends observed at College are similar to those observed at Watson Lake, that is, an increasingly stronger wind as the disturbance level increases representing a polar cap flow pattern. However, with the coarse College binning it is impossible to gauge the transition period when the neutral winds convert from a midlatitudinal style flow to a polar cap flow. Finally, the Watson Lake data set illustrates that it is difficult to characterize neutral winds at a transitional site with a harmonical relationship employing diurnal, semidiurnal, and higher-order terms, as was alluded to by *Faulkot et al.* [1993]. The combination of middle-latitude solar heating and high-latitude momentum transfer effects on the neutral wind flow should certainly be diurnally reproducible but may not easily be represented by tidal behavior except for the higher disturbance levels. In addition, there is a strong asymmetry be-

tween dusk winds and dawn winds at higher disturbance levels which results in a better developed vortex at dusk where the rotational Coriolis force assists the ion-drag forcing rather than opposing it at dawn [*Fuller-Rowell et al.*, 1984].

Regarding the Fabry-Pérot interferometer scans acquired while serendipitously observing aurora, the potential exists to use the wind and temperature information to characterize middle thermospheric altitudes. The altitude of peak emission of the O I (6300 Å) airglow feature is generally believed to originate from an altitude near or above 240 km, though the full width at half maximum of the emission is about 50 km [*Cogger et al.*, 1980]. Auroral electron precipitation of mean energies in the range 1 to 10 keV are preferentially stopped at middle thermospheric levels and in the process increase the plasma density which consequently supplies the dissociative recombination reaction producing O I (6300 Å) emission. The result, as may be simulated by the GLOW routine, is a decrease in the altitude of the peak volume emission rate for this feature. It is characteristic for the lower altitudes to be cooler than the upper thermosphere and if the neutral temperature associated with the Fabry-Pérot measurement is accurate, then it is possible to probe lower altitudes. Unfortunately, the Fabry-Pérot on its own, cannot distinguish the mean energy of the precipitation and, more seriously, may not easily discriminate against potential contaminating molecular auroral emissions which may also be recorded. The contaminant emission will act to either enhance the recorded background level between observed fringes, or actually mix with the airglow channel. Further spectral simulation studies are required to address these problems if true auroral observations are desired.

Conclusions

Observations of the thermospheric neutral winds at a transitional site near the auroral oval boundary were conducted for four different seasons between November 1991 and April 1993. The neutral wind data sets were ordered based upon the terrestrial geomagnetic disturbance level on an hourly basis.

1. For the lowest level of geomagnetic disturbance and the lowest level of solar activity, the horizontal neutral wind flow pattern is primarily controlled via solar heating in the form of a pressure gradient force. This is most evident in the December 1992 solstice data set ($F_{10.7}$ = 125) for K_p = 0 to 1.

2. For the higher levels of geomagnetic disturbance, the neutral wind flow pattern represents a polar cap flow driven primarily by momentum transfer from a rapidly moving ion flow. Dusk/dawn asymmetries arise from associated rotational forcing (Coriolis acceleration) resulting in a neutral flow which is highly tangential and anticlockwise in the dusk sector and less so in the dawn sector.

3. The VSH model formulation of the NCAR TGCM represents much of the horizontal neutral wind data correctly. Unfortunately, with the coarse 5°x5° latitude/longitude grid size, the finer details regarding the transition between midlatitude flow and polar cap flow are blended together. The correspondence between the VSH representation and the Watson Lake observations is best during cases of higher magnetic disturbance levels when the site resides within the auroral oval.

4. The O I (6300 Å) airglow signal level, in addition to being higher when the solar flux level is greater, also increases as the geomagnetic disturbance level increases. This is also simulated by the GLOW model. Cases of distinct auroral emission may eventually provide a diagnostic tool for probing the middle thermospheric levels.

The Fabry-Pérot interferometer experiment at Watson Lake has shown the potential for remotely observing the O I (6300 Å) airglow in an unattended, long-term fashion with current state-of-the-art hardware. A network of environmentally stable aeronomical observatories can provide a diagnostic tool for monitoring upper atmosphere thermodynamics in the same fashion as remote meteorological weather stations. The deployment of such a network would provide a mechanism to observe the solar and magnetospheric impact of "space weather" on the near-Earth environment and assist in the fine tuning of circulatory models which would aid in forecasting the same.

Acknowledgments. The authors are deeply appreciative for the gracious support from NSF through grant ATM-9002608 for the construction, deployment, and operation of the Watson Lake facility. Funding for the data analysis was provided through NSF grant ATM-9301867. Discussions with Alan Burns are also appreciated. Access to the VSH numerical model was possible with the helpful assistance of Heather Elliott and Trevor Gardner.

The Editor thanks R.W. Smith and M.J. Buonsanto for their assistance in evaluating this paper.

References

Aruliah, A. L., D. Rees, and T. J. Fuller-Rowell, The combined effect of solar and geomagnetic activity on high latitude thermospheric neutral winds, I, Observations, *J. Atmos. Terr. Phys.*, *53*, 467, 1991a.

Aruliah, A. L., D. Rees, and Å. Steen, Seasonal and solar cycle variations in high-latitude thermospheric winds, *Geophys. Res. Lett.*, *18*, 1983, 1991b.

Cogger, L. L., J. C. G. Walker, J. W. Meriwether, Jr., and R. G. Burnside, *F* region airglow: Are ground-based observations consistent with recent satellite results?, *J. Geophys. Res.*, *85*, 3013, 1980.

Crickmore, R. I., Mean thermospheric winds observed from Halley, Antarctica, *Ann. Geophys.*, *12*, 1101, 1994.

Dickinson, R. E., E. C. Ridley, and R. G. Roble, A three-dimensional general circulation model of the thermosphere, *J. Geophys. Res.*, *86*, 1499, 1981.

Fauliot, V., G. Thuillier, and M. Herse, Observations of the F-region horizontal and vertical winds in the auroral zone, *Ann. Geophys.*, *11*, 17, 1993.

Feldstein, Y. I., and G. V. Starkov, Dynamics of auroral belt and polar geomagnetic disturbances, *Planet. Space Sci.*, *15*, 209, 1967.

Fuller-Rowell, T. J., and D. Rees, A three-dimensional, time dependent, global model of the thermosphere, *J. Atmos. Sci.*, *37*, 2545, 1980.

Fuller-Rowell, T. J., D. Rees, S. Quegan, G. J. Bailey, and R. J. Moffett, The effect of realistic conductivities on the high-latitude neutral thermospheric circulation, *Planet. Space Sci.*, *32*, 469, 1984.

Gattinger, R. L., and A. Vallance Jones, Quantitative spectroscopy of the aurora, II, The spectrum of medium intensity aurora between 4500 and 8900 Å, *Can. J. Phys.*, *52*, 2343, 1974.

Hagan, M. E., A. Aruliah, M. A. Biondi, M. J. Buonsanto, M. L. Dubion, B. Fejer, C. G. Fesen, S. Fukao, A. E. Hedin, R. Niciejewski, W. L. Oliver, D. P. Sipler, and J. Thayer, Selected results of a coordinated analysis of the thermosphere (abstract), *20th General Assembly*, p. 199, IUGG, Vienna, 1991.

Hedin, A. E., M. A. Biondi, R. G. Burnside, G. Hernandez, R. M. Johnson, T. L. Killeen, G. Mazaudier, J. W. Meriwether, J. E. Salah, R. J. Sica, R. W. Smith, N. W. Spencer, V. B. Wickwar, and T. S. Virdi, Revised model of thermospheric winds using satellite- and ground-based observations, *J. Geophys. Res.*, *96*, 7657, 1991.

Holzworth, R. H., and C.-I. Meng, Mathematical representation of the auroral oval, *Geophys. Res. Lett.*, *2*, 377, 1975.

Killeen, T. L., and P. B. Hays, Doppler line profile analysis for a multichannel Fabry Perot interferometer, *Appl. Opt.*, *23*, 612, 1984.

Killeen, T. L., R. G. Roble, and N. W. Spencer, A computer model of global winds and temperatures, *Adv. Space Res.*, *7*, 207, 1987.

McCormac, F. G., T. L. Killeen, B. Nardi, and R. W. Smith, How close are ground-based Fabry-Perot thermospheric wind and temperature measurements to exospheric values? A simulation study, *Planet. Space Sci.*, *35*, 1255, 1987a.

McCormac, F. G., T. L. Killeen, J. P. Thayer, G. Hernandez, C. R. Tschan, J. J. Ponthieu, and N. W. Spencer, Circulation of the polar thermosphere during geomagnetically quiet and active times as observed by Dynamics Explorer 2, *J. Geophys. Res.*, *92*, 10133, 1987b.

Meriwether, J. W., Jr., C. A. Tepley, S. A. Price, P. B. Hays, and L. L. Cogger, Remote ground-based observations of terrestrial airglow emissions and thermospheric dynamics at Calgary, Alberta, Canada, *Opt. Eng.*, *22*, 128, 1983.

Mulligan, F. J., A new technique for the real-time recovery of Fabry Perot line profiles, *J. Phys. E Sci. Instrum.*, *19*, 545, 1986.

Niciejewski, R., T. L. Killeen, and M. Turnbull, Ground-based Fabry-Pérot interferometry of the terrestrial nightglow with a bare charge-coupled device: Remote field site deployment, *Opt. Eng.*, *33*, 457, 1994.

Sica, R. J., Auroral zone thermospheric dynamics using Fabry-Perot interferometric measurements of the OI 15867K emission, Ph. D. thesis, Univ. of Ala., Fairbanks, 1984.

Sica, R. J., M. H. Rees, G. J. Romick, G. Hernandez, and R. G. Roble, Auroral zone thermospheric dynamics, 1, Averages, *J. Geophys. Res.*, *91*, 3231, 1986a.

Sica, R. J., M. H. Rees, R. G. Roble, G. Hernandez, and G. J. Romick, The altitude region sampled by ground-based Doppler temperature measurements of the OI 15867 K emission line in aurorae, *Planet. Space Sci.*, *34*, 483, 1986b.

Solomon, S. C., Auroral electron transport using the Monte Carlo method, *Geophys. Res. Lett.*, *20*, 185, 1993.

Titheridge, J. E., Mean meridional winds in the ionosphere at 70°N, *Planet. Space Sci.*, *39*, 657, 1991.

T. L. Killeen and R. J. Niciejewski, Space Physics Research Laboratory, University of Michigan, 2455 Hayward St., Ann Arbor, MI 48109-2143 (e-mail: niciejew@caen.engin.umich.edu)

S. Solomon, LASP, University of Colorado, Boulder, CO.

(Received April 13, 1995; revised August 15, 1995;
accepted August 17, 1995.)